Macromolecules

Open Access

pubs.acs.org/Macromolecules

Article

Revival of Polyacetylenes in Electronics: Green Light-Emitting Diodes

Lukáš Petřkovský, Ivo Kuřitka, Jiří Zedník, Jiří Vohlídal, Vojtěch Nádaždy, Jakub Ševčík, David Škoda, Bita Ghasemi, Michal Urbánek, Barbora Hanulíková, and Pavel Urbánek*

Cite This: *Macromolecules* 2024, 57, 7808–7819

Read Online

ACCESS | Metrics & More | Article Recommendations | Supporting Information

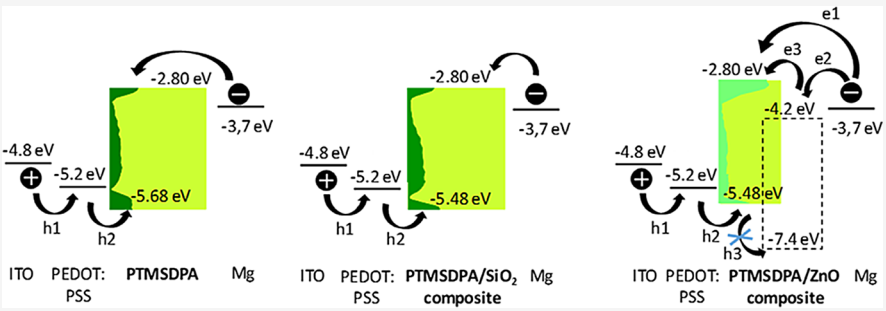

ABSTRACT: Polyacetylenes (PAs) are among the fundamental semiconducting polymers, but interest in them is currently waning due to the low stability under the workload of electronic devices made from them. Knowledge about the effect of substituents, additives, and fillers on the electronic structure of PA, which is closely related to the stability of these materials and related devices, is not at the required level either. This study deals with an air-stable PA, poly{1-[4-(trimethylsilyl)phenyl]-2-phenylacetylene} (PTMSDPA), and its composites with SiO_2 insulating nanoparticles and ZnO semiconducting nanoparticles. The electronic structures of these materials are analyzed by using energy-resolved electrochemical impedance spectroscopy (ER-EIS) and electron spectroscopic methods. The materials are used to construct electroluminescent diodes, the characteristics of which are presented. The results obtained demonstrate the positive effect of nanoparticle fillers on current efficiency and luminance (up to 182 cd/m^2, comparable to current displays) as well as on the stability and lifespan of the diodes with an active layer based on PTMSDPA nanocomposites compared to pure PTMSDPA.

INTRODUCTION

Several decades have passed since the first semiconducting poly(acetylene) (PA) films were prepared,[1] and by doping, they were transformed to materials with near-metal conductivity (10^4 to 10^5 S/cm).[2−4] At that point, poly(acetylene) became the prototype functional polymer for applications in electronics. Polymerization directly providing a PA film[1] usable for many applications has partly removed processing barriers stemming from the insolubility and infusibility of PA. However, it did not remove the low stability of PA under workload and especially in the air. Additionally, a weak luminescence intensity was another drawback of PA.[5−7]

The introduction of suitable side groups is a common strategy to improve unfavorable properties of a nonsubstituted polyacetylene and to modify its electronic structure. However, even substituted PAs did not bring a breakthrough in the field of polymer light-emitting diodes (PLEDs). They mostly showed a very low quantum yield of both photoluminescence and electroluminescence.[8] Another problem is their low stability in air, especially in solutions (i.e., during possible processing), where they can degrade quickly without any induction period[9] and undergo cis-to-trans isomerization changing their electronic properties.[10,11] Later, the development of synthesis procedures opened the way for tuning the band gap and improving the luminescence efficiency of substituted PAs. Another advantage of the synthetic processes' development is the significant extension of their luminescence to the blue region.[12−17] However, the low electroluminescence luminance of PAs-based devices that usually did not exceed 10 cd/m^2[14,15] has remained the limiting factor. The luminance of PAs was increased up to 1000 cd/m^2 by mixing them with other highly emissive polymers or by filling them with a luminescent dye.[12−19] The PA blend with improved hole conductivity showed luminance above 1000 cd/m^2, while the PA with carbazole side groups gave a value above 4200 cd/m^2.

Received: April 16, 2024
Revised: August 1, 2024
Accepted: August 5, 2024
Published: August 13, 2024

However, these high-luminance PA-based materials continued to struggle with low oxygen resistance[20] and low thermal and UV stability.[21,22] Hence, their application in organic-polymer-based electronics has remained doubtful.[23] Nevertheless, several other materials with similar deficiencies were remediated by different approaches (methods), thus opening a new opportunity for PAs as well. (i) Mixing the polymer with semiconducting inorganic nanoparticles (NPs) provided composites with better charge-carrier transport to recombination centers and thus increased luminance.[24,25] (ii) The supramolecular structure of the polymer can be altered through various methods, such as adjusting its molar mass,[26] annealing its layers,[27] or introducing a bulky filler that interferes with the regular conformations of polymer chains.[28]

Besides PAs for electronic applications, various poly(monosubstituted acetylene)[29] and poly(disubstituted acetylene)s with trialkylsilyl side groups were prepared, which have shown high stability in the air.[30,31] However, the use of these new materials was directed elsewhere, in the areas of gas/vapor separation membranes,[30,32] fluorescent and colorimetric sensors,[33] or, most recently, as a luminescent probe for plastic recycling.[34] In the present work, we took advantage of the stability of poly(diarylacetylenes) and choose poly[1-[4-(trimethylsilyl)phenyl]-2-phenyl-acetylene] with trialkylsilyl groups anchored on phenyl side groups (PTMSDPA, Figure 1) as the active polymer, which offers good solubility,

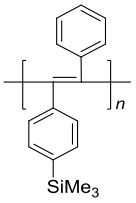

Figure 1. Structural formula of PTMSDPA.

easy processing, and bright luminescence.[32−34] PTMSDPA is a flexible tough polymer resistant to atmospheric oxygen, which is dominantly used as a material for gas separation membranes, especially for air enrichment with oxygen. The ability to create flexible rigid self-supporting foils is of course also welcome for materials with applications in optoelectronics.[35−37]

The effects of nanoparticles on these properties are studied on PTMSDPA nanocomposites with two fundamentally different NP fillers: insulating silicon dioxide (SiO_2) and semiconducting ZnO. Specimens of encapsulated PLEDs with active thin layers of these three materials are prepared, and their electroluminescence spectra, current efficiency, luminance, maximum luminance, and stability are investigated. The observed strong positive effects of the NPs on the performance of PLEDs correlate with data on the electronic structure characteristics of their active layers, which are obtained by energy-resolved electrochemical impedance spectroscopy (ER-EIS) and other optical spectroscopic methods. The ER-EIS method has recently proven to be a very powerful tool for studying the electronic structure of polymer thin films.[38] We believe that the demonstrated stability and acceptable efficiency of these devices will improve the reputation of polyacetylenes and revive interest in them as materials suitable for polymer electronics.

EXPERIMENTAL SECTION

Materials. 1-[4-(Trimethylsilyl)phenyl]-2-phenylacetylene 99% (TMSDPA) (TCI, Zwijndrecht, Belgium), tantalum(V) chloride ($TaCl_5$, 99.9%) (ABCR, Schlehert, Germany), tetrabutyltin (98%), toluene (anhydrous) and SiO_2 nanoparticles (all Merck KGaA, Sigma-Aldrich, Darmstadt, Germany), argon (Linde Praha), methanol, propan-2-ol, acetone, chloroform, toluene, and tetrabutylammonium hexafluorophosphate $TBAPF_6$ (all Lach:ner, Neratovice, Czech Republic) were used as supplied. Indium tin oxide (ITO) and quartz and glass substrates were supplied by Ossila, Sheffield GB. PEDOT:PSS (Clevios Al 4083) was used in this study and was delivered by Heraeus, Germany.

Synthesis of PTMSDPA. PTMSDPA (see Figure 1) was prepared by polymerization of TMSDPA catalyzed by the $TaCl_5/Bu_4Sn$ system under a dry argon atmosphere using a previously described procedure[36,37] (relative yield ∼100%, see Supporting Information for details). The obtained flexible yellow-orange solid polymer was reprecipitated three times to remove catalytic residues, and its relative molar mass characteristics $\langle M\rangle_{rw} = 5.2 \times 10^6$ and $Đ = 2.8$ were determined by the SEC method: Agilent 1100 HPLC chromatograph, series of three (mixed D, mixed C, and mixed B) PL-Gel columns (Polymer Laboratories. Bristol, UK), UV/vis detection at 254 nm, and THF eluent (0.7 mL/min).

Synthesis of ZnO Nanoparticles. Semiconducting ZnO nanoparticles were prepared by a microwave-assisted thermal decomposition of zinc acetate dihydrate in diethylene glycol (DEG) with the use of oleic acid as a capping agent according to the published procedure.[24,25] This facile method provides ZnO nanocrystals (5−12 nm) easily dispersible in nonpolar organic solvents (toluene and hexane), giving relatively highly concentrated colloidal solutions (0.07 M).[24]

Characterization of Nanoparticulate Fillers. The size and shape distributions of the fillers (see Figure S1) were determined by transmission electron microscopy (TEM) using a JEOL JEM 2100 microscope operated at 200 kV (LaB_6 cathode, point resolution 2.3 Å) equipped with an OLYMPUS SYS TENGRA camera (2048 × 2048 pixels). OLYMPUS Soft Imaging Solutions software was used to obtain the particle size distributions. Samples for TEM analyses were prepared by dropping ZnO and SiO_2 dispersions on carbon-coated copper grids (300 mesh), followed by drying at 80 °C for 1 h.

Preparation and Characterization of Thin Films. The PTMSDPA, PTMSDPA/ZnO, and PTMSDPA/SiO_2 films of appropriate thicknesses deposited onto different substrates (quartz glass, ITO-coated quartz glass, and ITO-coated quartz) were prepared by a spin-coating method using a Laurell WS-650-MZ-23 NPP instrument (2000 rpm in 30 s) and solutions of the mentioned materials in the chloroform/toluene (1/1 by vol) mixture. All substrates were cleaned by consecutive 10 min sonication in (i) distilled water with a Hellmanex cleaner, (ii) acetone, and (iii) propan-2-ol, and by successive UV ozone treatment for 10 min. The polymer concentration was always 2 mg/mL, and the NPs were added in the amount of 2.5 mg/mL (the resulting PTMSDMA/NPs mass ratio was 1:1.25). In order to prevent the effect of oxygen and moisture, all solutions, as well as spin-coated thin films, were prepared under argon in a glovebox. The thickness of the layers was measured with a mechanical profilometer with a resolution of 1 nm (Dimension ICON, Bruker, USA). Thicknesses of the prepared films for neat PTMSDPA were 45 ± 7 nm, PTMSDPA/SiO_2 were 35 ± 11 nm, and PTMSDPA/ZnO were 59 ± 8 nm. Surface analysis of the films was performed using the atomic force microscope dimension icon (Bruker, USA).

The UV−vis absorption spectra were recorded on a PerkinElmer Lambda 1050 spectrometer. Photoluminescence (PL) spectra were measured on a Fluorimeter FSL 920 instrument equipped with a high-voltage tungsten lamp (Edinburgh Instruments). Emission and excitation spectra corrected to the light source and detector spectral sensitivity. A standard L geometry was used with a single inclined specimen and an excitation light incidence angle of 55°. Measurements were performed in an evacuated cryostat (LN2 Optistat,

https://doi.org/10.1021/acs.macromol.4c00862
Macromolecules 2024, 57, 7808−7819

Oxford Instruments, UK). The PL quantum yield of the materials was determined using the method of absolute measurement in an integrating sphere with a diameter of 150 mm. Values are summarized in Table S1.

The innovative method of energy-resolved electrochemical impedance spectroscopy (ER-EIS) was used to obtain information about the distribution of electronic states (HOMO and LUMO) and defect states inside the prepared thin layers in the form of a so-called density of electronic state (DOS) map. The ER-EIS method is based on measurement of the resistance of the semiconductor/electrolyte interface R_{ct} during charge transfer induced by a sinusoidal voltage, where the redox process determines the real component of the impedance. The DOS function $g(E)$ in the semiconductor at the electrochemical potential $E_{F,redox} = eU$ is given by[39]

$$g(E_{F,redox} = eU) = \frac{1}{e^2 k_{et}[A]SR_{ct}} \quad (1)$$

where e is the elementary charge, U is the voltage at which R_{ct} was measured, k_{et} is the charge-transfer rate constant, $[A]$ is the concentration of redox active electrolyte species in the interphase region, and S is the contact area. The reciprocal value of R_{ct} is measured as a response to harmonic perturbation dU, and appropriate angular frequency ω provides direct information about the electronic DOS at the energy adjusted by an external voltage.

The ER-EIS experiments were performed on a Solartron analytical (model 1260) impedance/gain-phase analyzer. The AC harmonic voltage frequency was set to 0.5 Hz; the rms value of dU was 100 mV, and the average sweep rate of the DC voltage ramp was 10 mVs^{-1}. The measurements were performed in a glovebox with a protective N_2 atmosphere (oxygen <20 ppm; moisture <2 ppm) using a common three-electrode electrochemical cell with a volume of about 200 μL. The solution of 0.1 M $TBAPF_6$ in acetonitrile was used as the supporting electrolyte. The potential of the working electrode with respect to the reference Ag/AgCl electrode was controlled by a potentiostat. Pt wire was used as the counter electrode. The potential recorded with respect to the reference Ag/AgCl electrode can be recalculated to the local vacuum level, assuming the Ag/AgCl energy versus vacuum value of 4.66 eV.

Preparation and Characterization of PLED. The PLED devices with the studied active layers were prepared under a nitrogen atmosphere (glovebox JACOMEX GP Concept) as follows: PEDOT:PSS was filtered through a 0.45 μm PVDF filter and deposited as a hole transporting layer (HTL) onto purified standard patterned ITO substrates (Ossila Ltd., with six active pixels) by a standard procedure. Then, the active material layer was deposited onto the HTL layer by spin coating (1000 rpm) from its solution in toluene (100 μL). The layer was dried at 150 °C on a hot plate and covered by a magnesium cathode by using a Quorum Technologies Q300TT sputter-coater. Finally, the PLED device was encapsulated with an epoxy polymer.

The PLED performance (current−voltage-luminance characteristics) was measured by using Source Measure Unit (SMU) XTralien X100 (Ossila Ltd.). Electroluminescence spectra and intensities of PLEDs were measured using the integrating sphere (Avantes AvaSpec 2048 fiber spectrometer) with a powering voltage of 15 V supplied from the SMU. The current efficiency (CE) was obtained as the ratio of the luminance L_{vPLED}, obtained by Chroma Meter CS 150 (Konica Minolta), and the current density.

RESULTS AND DISCUSSION

UV/Vis and Room Temperature Photoluminescence Spectra Analysis of Thin Films. UV/vis absorption spectra (Figure S2) did not reveal any significant change upon adding fillers. The admixed SiO_2 NPs did not alter the spectrum of PTMSDPA at all. The admixed ZnO NPs increased the baseline of the spectrum on the whole spectral range due to light scattering with increasing intensity toward the blue end. However, the absorption features specific to ZnO NPs remained overlaid by the prominent absorption spectrum of the polymer. The UV/vis absorption spectra of all films showed the first absorption band apex at the wavelength $\lambda_{A,max}$ = 430 nm, which was used for excitation of photoluminescence (PL) spectra. A broad emission band with a maximum at 550 nm was observed (see Figure S3a) that is typical of the PTMSDPA.[31] The wavelength of the green emission maximum was not affected by added fillers. Similarly, the excitation spectra of the neat polymer and its nanocomposites recorded at an emission wavelength of 550 nm (Figure S3b) did not differ significantly from each other. Hence, it is clear that the polymer matrix dictates the spectral properties of all three materials.

The excitation PL spectra showed two bands corresponding to transitions to different vibrational states: at 430 nm (0−0 transition) and 375 nm (0−1 transition). In contrast, the emission spectra showed only one broad peak with a maximum at 550 nm, which breaks the well-known mirror image rule of the absorption and PL spectra. This testifies to the complete relaxation of the vibrational excited state S_{E1} to the ground vibrational level S_{E0} (energy decrease of about 0.45 eV), from which the radiative 0−1 transition to the S_{G1} level takes place. However, the observed Stokes shift of 0.63 eV (between 430 and 550 nm) is larger, indicating an additional contribution to the relaxation process. The reason for this can be seen in the variety of conformations of segments of conjugated macromolecules, which is manifested by a certain distribution of band gap energies in the respective conjugated polymer. In other words, HOMO and LUMO energy levels are closer or farther to/from each other on various segments, similarly as was reported for previously investigated systems.[40−43] If the mean band gap energy is, ca., 0.6 eV, its variation can be estimated, ca., 0.3 eV. Excitons diffuse along the polymer chain from the higher energy to lower energy sites until they decay by a radiant or nonradiant transition. The longer the travel, the deeper the energy relaxation achieved. Moreover, radiant tunneling can occur from states in the vicinity of the edge of the conduction band.[44] Thus, emitted higher energy photons should show a faster luminescence decay than photons with a lower energy. This hypothesis is in accord with the luminescence lifetimes τ determined for three different emission wavelengths (given in nm as the subscript) of the emission band: τ_{500} = 0.53 ns; τ_{550} = 0.81 ns; τ_{600} = 1.01 nm.

Unlike composites of other conjugated polymers,[45] the added fillers did not significantly affect either the excitation or emission PL spectra of the PTMSDPA matrix, which indicates that the fillers basically did not alter the band gap energy distribution in the matrix. This corresponds to a low conformational variability of PTMSDPA chains, in which each main chain carbon atom carries a bulky substituent (phenyl or 4-(trimethylsilyl)phenyl), which not only reduce overlaps of the main chain π-orbitals but also make the coiled chain conformations inaccessible and chain packing irregular and loose, resulting in the unprecedentedly large free volume of this polymer, F'= 0.26.[46] Hence, conjugation over at most a few mers can be expected, and the local variability in configuration and conformation of the bulky side groups can significantly contribute to the observed energy level distributions.

The optical properties of PTMSDPA correspond to its structure, which is neither stereospecific in terms of E/Z isomerism of the main chain double bonds nor regioregular (head-to-tail). Therefore, no specific regular zigzag or helical

https://doi.org/10.1021/acs.macromol.4c00862
Macromolecules 2024, 57, 7808−7819

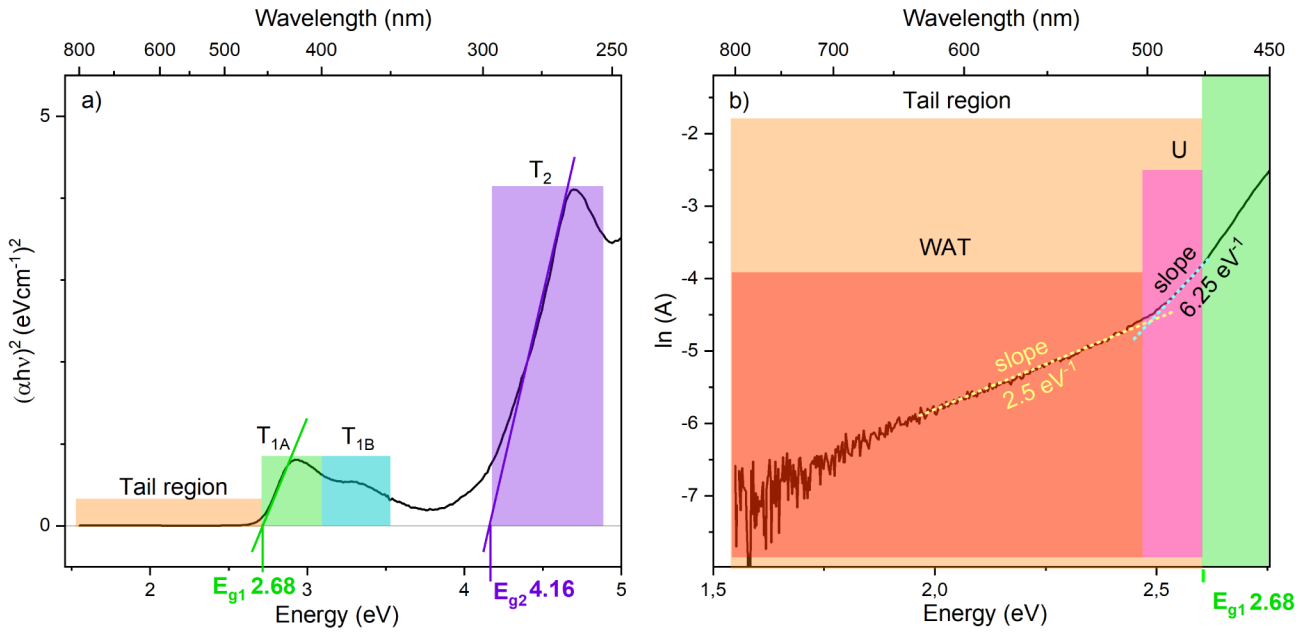

Figure 2. (a) Tauc plot for direct allowed transitions and (b) absorption spectrum in the logarithm scale replotted against absorbed light energy for band gap tail analysis, where U represents the Urbach tail region, WAT stands for the weak absorption transition region, T_{1A} indicates the region corresponding to the linear part of the Tauc plot (optical band gap E_{g1}) and 0−0 absorption and excitation band at around 435 nm (2.85 eV), T_{1B} indicates transitions related to the 0−1 absorption and excitation band situated at around 375 nm (≈3.30 eV), and T_2 refers to the second band gap region (E_{g2}). Corresponding electronic transitions are assigned to the prominent part of the spectrum.

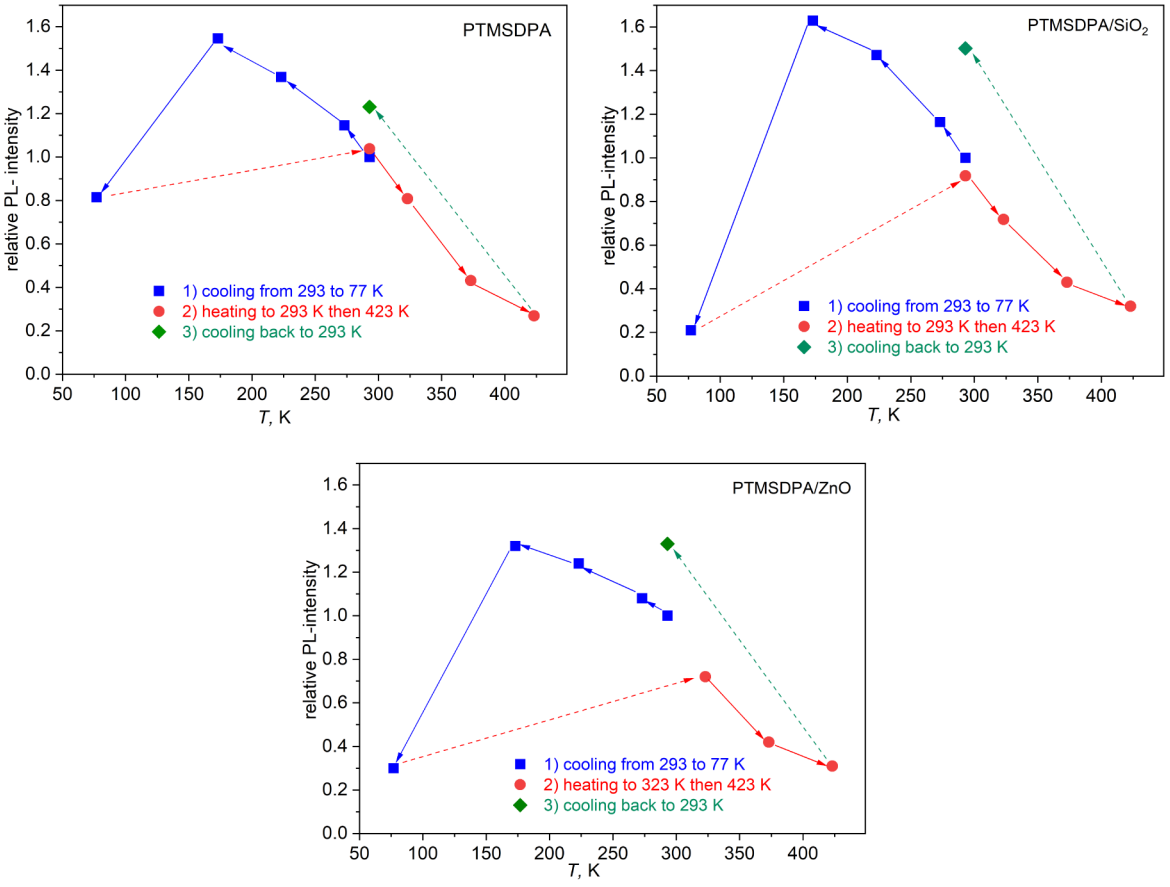

Figure 3. Changes in the relative PL intensity I_{PL} of studied films accompanying their stepwise thermal treatment are insinuated inside diagrams. The reference intensity (in 10^3 counts) of I_{PL} is 580 (PTMSDPA), 105 (PTMSDPA/SiO_2), and 100 (PTMSDPA/ZnO).

https://doi.org/10.1021/acs.macromol.4c00862
Macromolecules 2024, 57, 7808−7819

structures assembled in a crystalline phase can be expected, and this polymer can be classified as an amorphous material of the disordered semiconductor type. Thus, we evaluated band edges and the optical gap of the polymer in the form of a solid thin film using Tauc's plot and Urbach's tail analysis of the UV/vis absorption spectrum (Figure 2) to obtain an insight into the electronic structure of PTMSDPA. The Tauc plot is considered as a suitable tool for band gap analysis of such materials.[47−49] In Figure 3a, the best linear fit yields E_{g1} = 2.68 eV for allowed direct transitions between the valence band (VB) and the conduction band (CB). The linear part of the spectrum in the T_{1A} region spans approximately up to 2.85 eV (435 nm). At 2.88 eV (430 nm), a peak maximum is observed in the absorption spectra, which corresponds to the first maximum in the excitation spectrum associated with the $S_{G0} \rightarrow S_{E0}$ transitions. The second peak identified in the excitation spectrum as belonging to the $S_{G0} \rightarrow S_{E1}$ transition is clearly manifested in the region T_{1B} of the absorption spectrum at 3.30 eV (375 nm). A distinct second region T_2 in the absorption spectrum, which is well-separated from the T_1 region, has a well-defined maximum at 4.70 eV (264 nm). This feature can be associated with another set of direct allowed transitions from lower-lying valence bands with an edge situated at, ca., E_{g2} = 4.16 eV.

On the other hand, the absorption edge of PTMSDPA is not abrupt due to the disorder of polymer coils. The corresponding analysis is depicted in Figure 2b. The absorption tail extends into the forbidden gap, which is manifested at lower energies (<2.68 eV). The first strictly linear part of this tailing region in the ln(A) plot was identified as the Urbach tail (U region) in the range 2.60−2.49 eV (477−498 nm). The second strictly linear region is found above 504 nm (below 2.46 eV) which is assigned as a weak absorption tail (WAT)[48,50−53] (Figure 2b). Although developed initially for inorganics, the Urbach tail and WAT analysis are also suitable for organic materials.[54]

The Urbach tail is associated with disorder, structural defects, and thermal vibrations in the material. Corresponding transitions are generally considered to be more likely from localized electronic states to extended states than from extended states to localized states. The Urbach tail region can be analyzed by plotting ln(A) versus photon energy ($h\nu$) in Figure 2b. The following equation describing the dependence of the absorbance (A) on the ($h\nu$) can be used to estimate the Urbach energy (E_U):[50]

$$A(h\nu) \sim e^{h\nu/E_U} \quad (2)$$

Thus, E_U was calculated as the reciprocal value of the slope of the linear fit to the corresponding part of the data indicated by the short dot line in Figure 2b. The value of the Urbach energy E_U = 0.16 eV obtained for the PTMSDPA thin film indicates a structural disorder of the polymer chains and distribution of localized states near the band gap edges.

The long wavelength part of the absorption spectrum belongs to the WAT region and is related to the imperfections of the material structure. Transitions between localized defect states are involved in this region. It can be analyzed using the following dependency of the absorbance (A) on the photon energy ($h\nu$):[50]

$$A(h\nu) \sim e^{h\nu/E_{WAT}} \quad (3)$$

The reciprocal value of the slope of the corresponding linear part of the ln(A) plotted versus ($h\nu$) gives the value of the weak absorption tail energy (E_{WAT}). E_{WAT} is always larger than E_U. The linear fit is indicated with a short dot line in Figure 2b. From its slope, a value of E_{WAT} = 0.40 eV was obtained. It suggests the presence of deep band gap states and localized tail state populations in the electronic structure of the examined PTMSDPA thin film.

Temperature-Dependent Photoluminescence Analysis. Kwak et al.[55] revealed a decrease in the PL intensity of PTMSDPA as its temperature increased and showed reversible periodic changes in its PL intensity when alternating its temperature between 273 and 363 K (20 and 90 °C). Since temperature effects are important for electroluminescent devices, we thoroughly examined the PL behavior of the studied materials in a wide temperature range. The measured PL spectra series is shown in Figure S4, and changes in relative PL intensity with respect to the initial value at 293 K (IPL) read from these spectra are shown in Figure 3. The PL spectra were first measured at gradually decreasing temperatures: at 293, 273, 223, 173, and 77 K (blue squares and arrows in Figure 4). Then, the film was tempered to and remeasured at

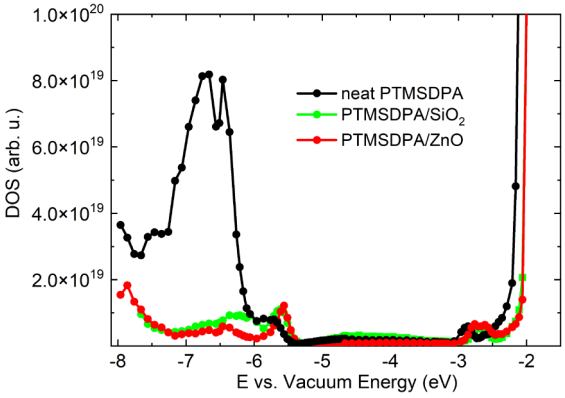

Figure 4. Representative linear scale ER-EIS spectra of prepared thin films.

293 K and further measured at temperatures of 323, 373, and 423 K (red circles and arrows). Finally, the film was cooled and measured again at 293 K (green square and arrow).

Obviously, Figure 3 shows that the PL intensity of all materials monotonically decreases with increasing temperature in the interval from 173 to 423 K, while the position of the emission band does not change (Figure S3). This well corresponds to the related results of Kwak et al.,[55] except that the I_{PL} changes with temperature observed here with temperature were not fully reversible. A significant increase in I_{PL} at 293 K has been observed if the material was gradually heated and tempered for a certain time to 323, 373, and 423 K (each step lasted 30 min) and then cooled back to 293 K (see differences between green and blue points in Figure 3). The I_{PL} increase indicates that the applied thermal treatment induced conformational changes in PTMSDPA molecules that resulted in their new packing, providing materials with an increased luminescence efficiency.

What is really new is the deep drop in I_{PL} when the emitting material is cooled from 173 to 77 K. The smallest drop showed neat PTMSPDA (50%, from 1.6 to 0.8), medium PTMSPDA/ZnO (79%, from 1.4 to 0.3), and the highest PTMSPDA/SiO_2 (87%, from 1.6 to 0.2). It is clear that this drop cannot be attributed to ongoing conformational changes in PTMSDPA molecules, which will not be possible at such low temperatures.

https://doi.org/10.1021/acs.macromol.4c00862
Macromolecules 2024, 57, 7808−7819

The excitons present in organic low-permittivity organic materials are of the Frenkel type. They are strongly bound due to low electrostatic shielding, with radii comparable to lattice spacing.[56] When conformational transformations freeze, interchain exciton transfers become difficult. Exciton diffusion will, therefore, gradually decrease, thereby increasing the influence of exciton−phonon interactions, by which the excitation energy is dominantly nonradiatively changed to the energy of lattice vibrations.[56]

Density of States Mapping of Solid Thin Films. The ER-EIS method was used for a detailed analysis and description of the band structure of thin polyacetylene and polyacetylene-matrix nanocomposite films for the first time. The linear-scale DOS functions for PTMSDPA and its ZnO and SiO_2 nanocomposites determined by the ER-EIS technique are compared in Figure 4. Besides nanoparticle addition, phase separation can affect the electric transport in sandwich devices. Therefore, we analyzed the homogeneity of prepared films, no phase separation was revealed, and good homogeneity was confirmed (see Figure S5). The bands at about −5.5 eV should be assigned to HOMO levels that are associated with the orbitals of the conjugated main chains. The lower-lying bands (range from −8 to −6 eV) are associated with the orbitals localized on aromatic side groups. In this region, both nanocomposites showed the DOS function about an order of magnitude smaller than that of neat PTMSDPA, which can be attributed to the interactions of phenyl groups with the polar surfaces of nanoparticles of both types. A similar decrease in DOS population indicates that it is a nonspecific effect of fillers with ionic surfaces.

A DOS function in the semilogarithmic scale rotated by 90° clockwise correlates to the electronic structure in the UV/vis and PL spectral bands (Figure 5). Absorption transitions are indicated by light blue, excitation transitions by dark blue, and emission transitions by green arrows.

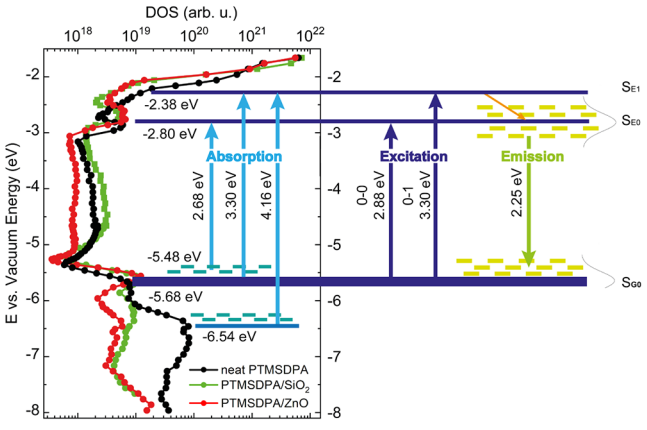

Figure 5. Representative logarithmic scale ER-EIS spectra of prepared thin films along with the Jablonski diagram.

If value 5.68 eV is assigned to the energy of the ground state (S_{G0} ≈ HOMO), then value −2.80 eV belongs to zero (S_{E0} ≈ LUMO) and value −2.38 eV to the first (S_{E1}) vibrational level of the first excited state. It can be seen from the DOS diagrams that the HOMO and LUMO levels of nanocomposites are slightly higher (about, ca., 0.15 eV) compared to the corresponding levels of the neat PTMSDPA. This observation can also be attributed to the abovementioned nonspecific effect of fillers with polar surfaces. As the neat polymer and its composites practically showed the same band gap energy, this shift does not affect the correlation between spectral bands and the DOS diagram.

The corresponding transitions T_{1A} = 2.88 eV and T_{1B} = 3.30 eV in the UV/vis spectrum (see Figure 3a), and the value E_{g1} = 2.68 eV estimated from the Tauc plot can be identified. The value ofE_{g2} = 4.16 eV may specify the onset of the transitions associated with the T_2 region in the UV/vis spectrum to the states below −6.54 eV. Excited electrons may reach either higher vibrational levels of LUMO or above LUMO lying empty orbitals. There is almost no difference between the UV/vis spectra of PTMSDPA and PTMSDPA/(SiO_2 or ZnO), whereas there is a big difference between the populations of electronic states below −6 eV. Thus, the T_2 region with the T_2 maximum at 4.70 eV (264 nm) may be associated with the absorptions from HOMO or near below HOMO states to the higher-lying LUMO + n states.

As already mentioned, the 0−0 and 0−1 transitions in the excitation PL spectrum indicated by dark blue arrows in Figure 5 can be attributed to the states located at −5.68 eV (S_{G0}), −2.80 eV (S_{E0}), and −2.38 eV (S_{E1}). The $S_{E0} \rightarrow S_{G0}$ emission at 550 nm with a transition energy of 2.25 eV is indicated with the green downward arrow. It is set to the middle of the gap between S_{G0} and S_{E0} of the horizontal yellow dashed lines, indicating the distribution of the states as obtained by analysis of the PL spectra. The width of these distributions corresponds to 0.3 eV below LUMO and above HOMO. The orange arrow pointing obliquely downward indicates the energy relaxation processes involved in the excited state.

A note can be made on the width of the lines presented as S_{G0}, S_{E0}, and S_{E1} levels. Each of these energy levels can be considered ±0.3 eV wide, at least when considering de-excitation. On the other hand, the distribution width of levels representing the energy states associated with the absorption events, including excitations leading later to a photon emission, must be sharper, as there is no relaxation mechanism preferentially populating low-lying extremes. It can be assumed that it should be at most comparable with or less than the value of the Urbach energy, which is a manifestation of another certain disorder related to the near-edge states. Then, a value from ±0.1 eV to ±0.15 eV would be a sober guess.

The analysis of the Urbach tail revealed the value of E_U = 0.16 eV. It can be most likely associated with the distribution of localized states near above the edge of HOMO and transitions to LUMO. These states are indicated by horizontal light blue dash lines in Figure 5 near the beginning of the arrow corresponding to the transition from −5.48 eV to S_{E0} (attributed to E_{g1}). The WAT corresponding states are not indicated in Figure 5, but these transitions between deep localized states in the band gap can be attributed to the region between −3.0 and −5.4 eV. Indeed, the population of deep states in the forbidden gap is high in PTMSDPA unlike in other conducting polymers.[41−43,57] It can be ascribed to the enormous polymer coil disorder inherent to the structure of PTMSDPA with bulky side groups lacking stereospecificity (*E*/*Z* isomerism of substituents) and regioregularity (head-to-tail). The addition of SiO_2 fillers only slightly increases population density in this region, possibly provoking an increase in the disorder of the polymer matrix in the nanocomposite. On the other hand, the addition of ZnO fillers diminished the population of deep states in the forbidden gap, especially between −3.7 and −5 eV. This can be associated with an interaction between these states in the polymer forbidden gap

https://doi.org/10.1021/acs.macromol.4c00862
Macromolecules 2024, 57, 7808−7819

and the conduction band of ZnO lying at, ca., −4.2 eV,[58] which can heal defect localized deep states. It implies an electronic (charge transfer) interaction that overbalances the eventual weak general effect of disordering of the polymer matrix that is already inherently highly disordered. This is the fourth effect of the filler addition to the PTMSDPA matrix besides the significant depreciation of state density below −6 eV, slight PTMSDPA disordering, and the general shift of all energy levels by 0.15 eV.

Performance and Characterization of PLED. The current−voltage ($I-V$) characteristics of prepared PTMSDPA-based PLEDs are presented in Figure 6. The $I-V$ curves characteristically display a decrease in the opening bias with the polymer−nanoparticle composite as compared to the neat polymer-based device. The opening bias of the neat PTMSDPA device is around 15 V, and that of PTMSDPA/SiO_2 is approximately 8 V. PLED devices with ZnO nanoparticles exhibited an opening bias of about 10 V.

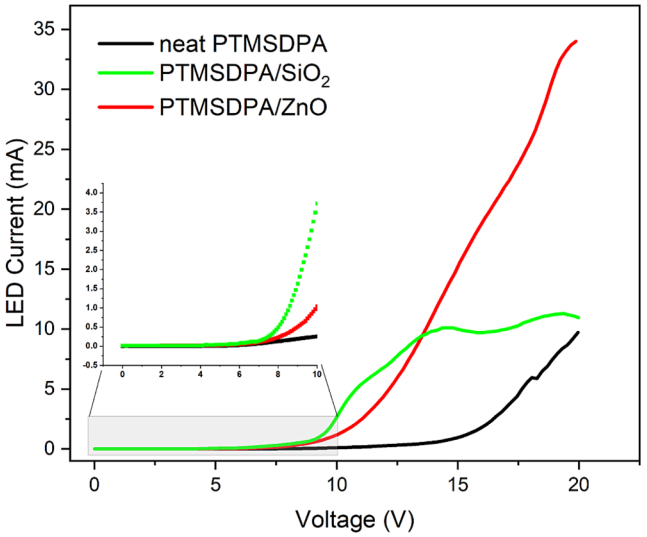

Figure 6. $I-V$ characteristics of the prepared devices.

The electroluminescence spectra of the PTMSDPA-based devices are plotted in Figure 7. Similarly to PL, the electroluminescence emission spectrum consists of only one broad peak with the maximum at about 545 nm and a very small deviation (around 5 nm).

To analyze and discuss the performance of the prepared devices, their parameters should also be expressed in terms of luminance and current efficiency. Such an approach enables comparison of the performance of prepared PLEDs with data reported in the past. Luminance and current were measured as the voltage gradually increased to the point where a short circuit and destruction of the diode occurred. Thus, the maximum achievable luminance and also the maximum electrical load (i.e., maximal voltage and electric current) of diodes were measured.

The obtained parameters for all prepared and tested samples are summarized in Table 1. The prepared sample set and individual devices can be ranked easily using the current efficiency, which is a value describing the luminance improvement of devices with a nanocomposite active layer compared to the devices based on the neat polymer active layer. The addition of any nanoparticles always resulted in an improved performance. In the case of SiO_2 nanoparticles, a maximal

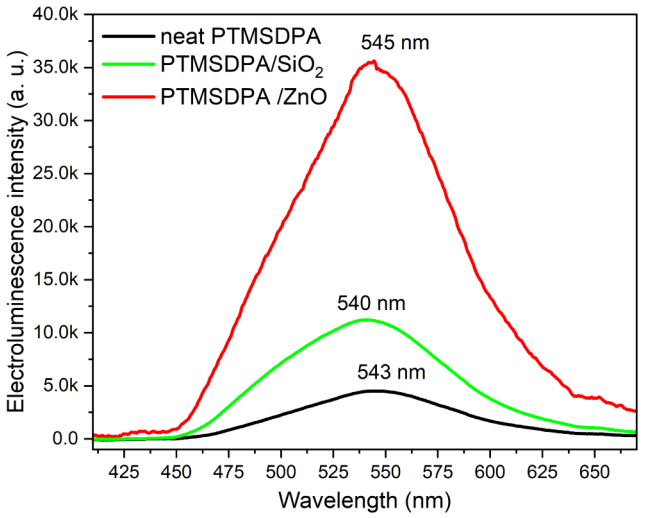

Figure 7. Electroluminescence spectra of the prepared devices operating at 15 V.

Table 1. Maximal Measured luminance Values, Current Density, and Current Efficiency from Obtained Data Calculated at the Point of the Highest luminance

PLED	opening bias [V]	maximal luminance [cd/m^2]	current density [mA/cm^2]	current efficiency [cd/A]
neat PTMSDPA	15	38	93	0.04
PTMSDPA/SiO2	8	182	273	0.07
PTMSDPA/ZnO	10	121	64	0.19

luminance of, ca., 180 cd/m^2 was achieved, which represents approximately the same luminance level as conventional PC screens or smartphone displays.[59] It is not only the maximal luminance that is an important parameter. The analysis of results achieved during the performance measurement of diodes depending on electrical quantities (power, current, and voltage) brings very interesting findings.

Figure 8 shows the dependence of the luminance on electrical quantities and the current efficiency dependence on the luminance. In case of all active layer types, the luminance increases linearly with increasing supplied electric power.

To achieve a comparable luminance of 120 cd/m^2, diodes with the PTMSDPA/ZnO active layer need about three times less electrical power than diodes with the PTMSDPA/SiO_2 active layer. If we extrapolated the performance of pure polymer diodes to 120 cd/m^2 luminance, then about five times more electric power would be needed compared to PTMSDPA/ZnO.

In the case of SiO_2 nanoparticles, it is evident that the current efficiency of diodes did not increase dramatically compared to that of the pure polymer. However, it was observed that the diodes filled with SiO_2 were able to carry a higher current load, which resulted in a higher luminance. It can be concluded that SiO_2 nanoparticles do not contribute to the transfer or recombination of charges in the active layer but rather have a stabilizing effect on the polymer matrix. This is highly likely due to their nonconductive nature. This is also evidenced by the dependence of the current efficiency on the luminance of neat polymers and polymer/SiO_2 devices (Figure 8d).

The situation is slightly different in the case of diodes with an active layer of PTMSDPA/ZnO. In this case, semi-

https://doi.org/10.1021/acs.macromol.4c00862
Macromolecules 2024, 57, 7808−7819

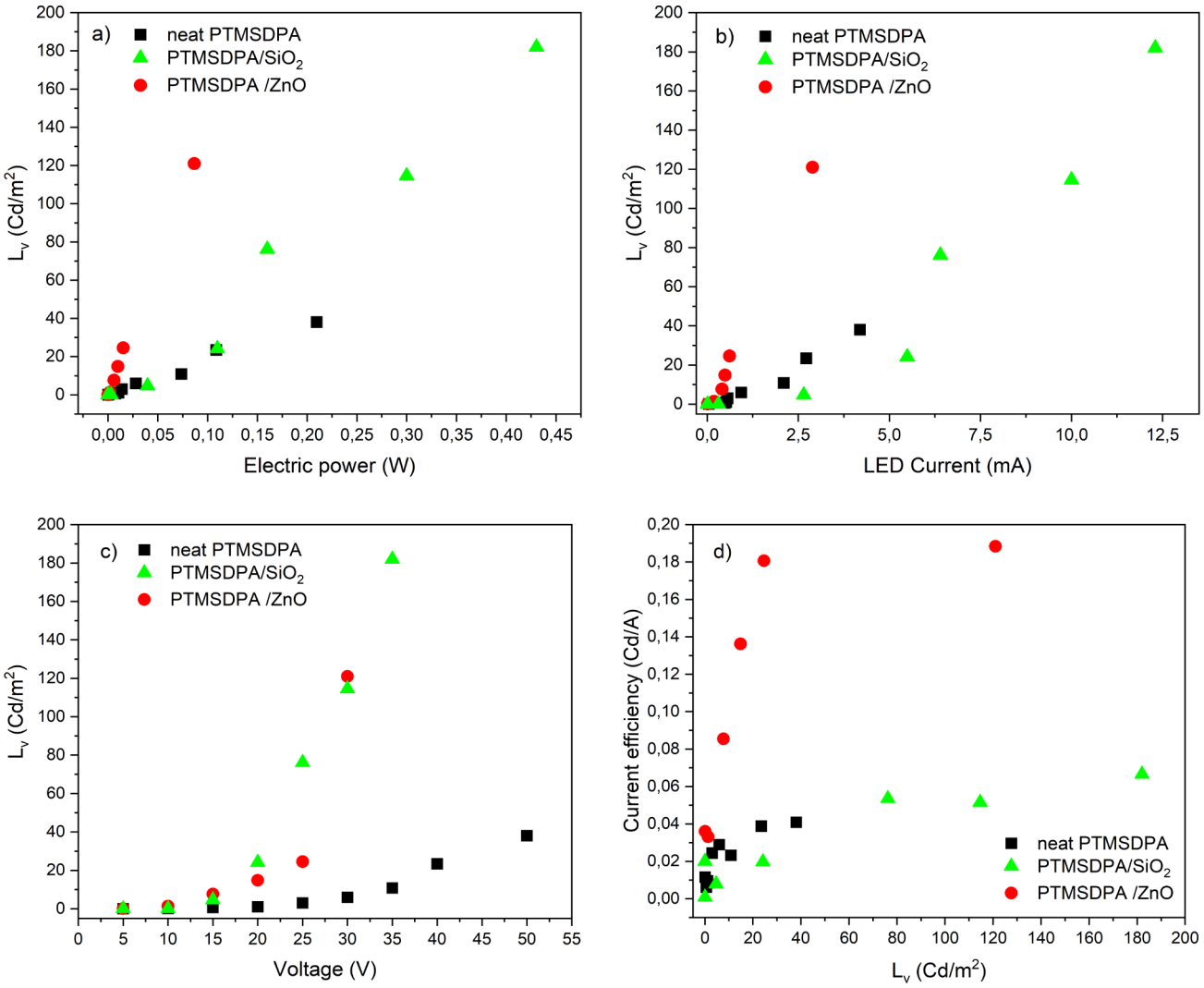

Figure 8. Luminance of prepared devices depending on (a) electric power, (b) electric current, and (c) voltage. (d) Dependence of current efficiency on luminance.

conducting ZnO nanoparticles cause a significant increase in the current efficiency (roughly 5-fold) compared to pure polymer diodes. The significant current efficiency increase is certainly due to the optimal level of the LUMO level of ZnO (−4.2 eV), which allows an easier transfer of electrons from the magnesium cathode to the active layer.[58] Also, the limitation of defect states in the band gap of the polymer matrix can also play a role, as can be seen in Figure 5.

The addition of nanoparticles to the polymer matrix has another interesting effect. As the electrical power of the diode increases, the chromaticity of the emitted light shifts to the green region in the case of active layers containing nanoparticles. In the case of the neat matrix, the chromaticity of the emitted light shifts more to the yellow region. This effect is shown in Figure 9, along with photographs of real diodes in operation.

An important criterion that we tested was the long-term operational stability of the prepared diodes. This testing was done by maintaining a constant current (0.05 mA) in the diodes and monitoring the voltage to compensate for the current drop. The results of this testing approach are summarized in Figure 10.

As with the improved luminance and current characteristics, diodes with composite layers showed a significant improvement over diodes with a pure polymer active layer. For pure PTMSDPA diodes, the compensating voltage increased from the initial voltage of 6 V at the beginning of the experiment to about 8 V at the end of the experiment. The total operating time of lighting during the experiment was 90 min. In contrast, diodes with the active layer filled with nanoparticles initially showed a lower bias (about 5.5 V) to reach the same current. This is in accordance with results from $I-V$ measurements, where the opening bias of diodes with a filled active layer is lower than the opening bias of pure PTMSDPA-based diodes. In the case of diodes with an active layer made of PTMSDPA/SiO_2, the compensation voltage decreases, and after 60 min, it stabilizes below the value of 5 V. In diodes with the PTMSDPA/ZnO active layer, the compensation voltage increases only very slightly and remains constant after 60 min of the experiment.

CONCLUSION

The presented results reliably indicate that the air-stable film-forming polyacetylene, which is free of the −CH═ main chain units, PTMSDPA, can be effectively used in electronics as an

https://doi.org/10.1021/acs.macromol.4c00862
Macromolecules 2024, 57, 7808−7819

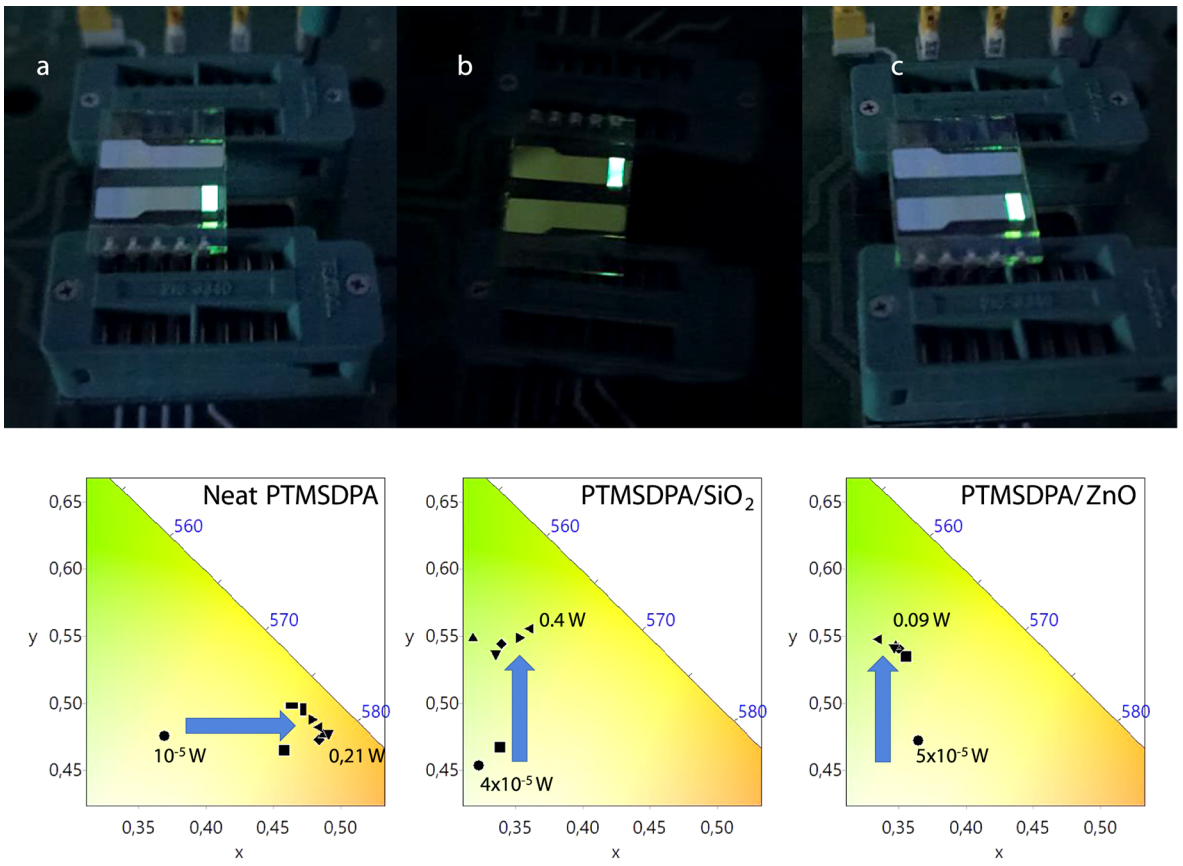

Figure 9. Pictures of prepared diodes (a) neat PTMSDPA, (b) PTMSDPA/SiO_2, and (c) PTMSDPA/ZnO and their chromacities depending on electric power.

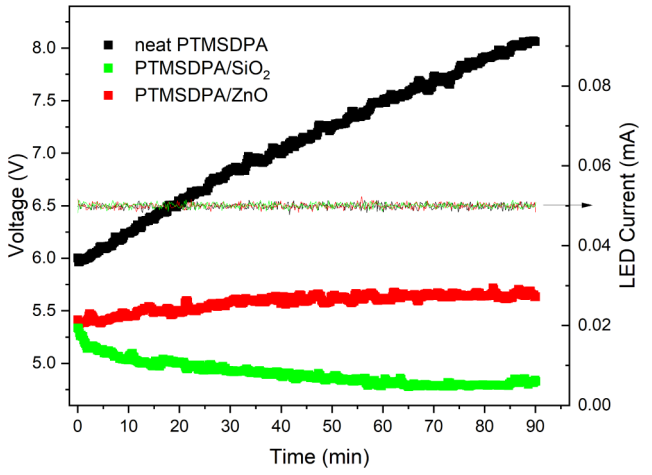

Figure 10. Dependence of the compensation voltage on time during the operation of the prepared diodes.

active material of electroluminescent diodes emitting green light, especially when applied as a matrix of nanocomposite layers. The insulating, light nonabsorbing nanofiller, SiO_2 has been proven to improve the luminous performance of this polymer to a level comparable to LEDs of common computer screens, while the semiconducting nanofiller, ZnO, has considerably increased the current efficiency of the light-emitting diode. Remarkable is the fact that with increasing power, the chromaticity of the PTMSDPA-LED shifts to yellow, while in the case of both types of composite LEDs, it shifts to green. The band structure mapping of the films of PTMSDPA and its nanocomposites by the ER-EIS method (used in this work for the first time to analyze polyacetylene-type films) revealed interesting effects of added fillers, in particular a significant reduction of the density of the states below −6 eV and a general upward shift of all energy levels by 0.15 eV.

We strongly believe that this work will help to restore interest in polyacetylenes as suitable materials for electronics.

■ ASSOCIATED CONTENT

Supporting Information

The Supporting Information is available free of charge at https://pubs.acs.org/doi/10.1021/acs.macromol.4c00862.

Detailed description of PTMSDPA synthesis; transmission electron microscopy characterization of used nanofillers; supporting spectroscopic data; AFM surface micrographs (PDF)

■ AUTHOR INFORMATION

Corresponding Author

Pavel Urbánek − *Centre of Polymer Systems, University Institute, Tomas Bata University in Zlín, Zlín 76001, Czech Republic;* orcid.org/0000-0002-9090-4681; Email: urbanek@utb.cz

Authors

Lukáš Petřkovský − *Centre of Polymer Systems, University Institute, Tomas Bata University in Zlín, Zlín 76001, Czech Republic*

https://doi.org/10.1021/acs.macromol.4c00862
Macromolecules 2024, 57, 7808−7819

Ivo Kuřitka − *Centre of Polymer Systems, University Institute, Tomas Bata University in Zlín, Zlín 76001, Czech Republic;* orcid.org/0000-0002-1016-5170
Jiří Zedník − *Department of Physical and Macromolecular Chemistry, Faculty of Science, Charles University, Prague CZ-128 40, Czech Republic;* orcid.org/0000-0001-7325-8684
Jiří Vohlídal − *Department of Physical and Macromolecular Chemistry, Faculty of Science, Charles University, Prague CZ-128 40, Czech Republic;* orcid.org/0000-0002-9412-2548
Vojtěch Nádaždy − *Institute of Physics, Slovak Academy of Sciences, Bratislava SK-845 11, Slovakia;* orcid.org/0000-0003-4127-5249
Jakub Ševčík − *Centre of Polymer Systems, University Institute, Tomas Bata University in Zlín, Zlín 76001, Czech Republic*
David Škoda − *Centre of Polymer Systems, University Institute, Tomas Bata University in Zlín, Zlín 76001, Czech Republic;* orcid.org/0000-0002-3787-1956
Bita Ghasemi − *Centre of Polymer Systems, University Institute, Tomas Bata University in Zlín, Zlín 76001, Czech Republic*
Michal Urbánek − *Centre of Polymer Systems, University Institute, Tomas Bata University in Zlín, Zlín 76001, Czech Republic*
Barbora Hanulíková − *Centre of Polymer Systems, University Institute, Tomas Bata University in Zlín, Zlín 76001, Czech Republic;* orcid.org/0000-0002-8300-0588

Complete contact information is available at: https://pubs.acs.org/10.1021/acs.macromol.4c00862

Author Contributions

L.P. contributed to investigation and visualization. I.K. contributed to data curation, formal analysis, funding acquisition, methodology, supervision, writing of the original draft, writing of review, and editing. J.iZ. contributed to data curation, formal analysis, investigation, writing of the original draft, writing of review, and editing. J.V. contributed to data curation, formal analysis, visualization, writing of the original draft, writing of review, and editing. V.N. contributed to data curation, formal analysis, investigation, validation, visualization, writing of the original draft, writing of review, and editing. J.Š. contributed to data curation and investigation. D.Š. contributed to data curation, investigation, and visualization. B.G. contributed to investigation. M.U. contributed to investigation. B.H. contributed to investigation and writing of the original draft. P.U. contributed to conceptualization, data curation, formal analysis, investigation, methodology, supervision, visualization, writing of the original draft, writing of review, and editing.

Funding

I.K., J.Š., D.Š., M.U., B.H., and P.U. acknowledge the University Institute at Tomas Bata University in Zlín and the Centre of Polymer Systems for financial support from the DKRVO funds (RP/CPS/2024-28/007). B.G. specifically acknowledges funding by the Internal Grant Agency of Tomas Bata University in Zlín, grant no. IGA/CPS/2024/002. V.N. also thanks the project VEGA No. 2/0165/22.

Notes

The authors declare no competing financial interest.

REFERENCES

(1) Shirakawa, H.; Ikeda, S. Infrared Spectra of Poly(Acetylene). *Polymer J.* **1971**, *2* (2), 231−244.
(2) Shirakawa, H.; Louis, E. J.; MacDiarmid, A. G.; Chiang, C. K.; Heeger, A. J. Synthesis of Electrically Conducting Organic Polymers: Halogen Derivatives of Polyacetylene, (CH)x. *J. Chem. Soc., Chem. Commun.* **1977**, No. 16, 578−580.
(3) Chiang, C. K.; Druy, M. A.; Gau, S. C.; Heeger, A. J.; Louis, E. J.; MacDiarmid, A. G.; Park, Y. W.; Shirakawa, H. Synthesis of Highly Conducting Films of Derivatives of Polyacetylene, (CH)x. *J. Am. Chem. Soc.* **1978**, *100* (3), 1013−1015.
(4) Park, Y. W.; Heeger, A. J.; Druy, M. A.; MacDiarmid, A. G. Electrical Transport in Doped Polyacetylene. *J. Chem. Phys.* **1980**, *73* (2), 946−957.
(5) Mele, E. J. Hot Luminescence in Polyacetylene. *Solid State Commun.* **1982**, *44* (6), 827−831.
(6) Yoshino, K.; Hayashi, S.; Sakai, T.; Inuishi, Y.; Kato, H.; Watanabe, Y. Photoluminescence of Polyacetylene in near Infrared. *Jpn. J. Appl. Phys.* **1982**, *21* (10), L653−L654.
(7) *Conjugated Polymers*, Reynolds, J. R.; Thompson, B. C.; Skotheim, T. A., Eds.; CRC Press, 2019. DOI: .
(8) Sun, R.; Masuda, T.; Kobayashi, T. Green Electroluminescent Emission from Substituted Polyacetylenes. *Jpn. J. Appl. Phys.* **1996**, *35* (11A), L1434.
(9) Vohlídal, J.; Kabátek, Z.; Pacovská, M.; Sedláček, J.; Grubišic-Gallot, Z. Size Exclusion Chromatography of Substituted Acetylene Polymers: Effect of Autooxidative Degradation of the Polymer During the Analysis. *Collect Czechoslov Chem. Commun.* **1996**, *61* (1), 120−125.
(10) Sedláček, J.; Vohlídal, J. Controlled and Living Polymerizations Induced with Rhodium Catalysts. A Review. *Collect Czechoslov Chem. Commun.* **2003**, *68* (10), 1745−1790.
(11) Bondarev, D.; Zedník, J.; Plutnarová, I.; Vohlídal, J.; Sedlaček, J. Molecular Weight and Configurational Stability of Poly-[(Fluorophenyl)Acetylene]s Prepared with Metathesis and Insertion Catalysts. *J. Polym. Sci. A Polym. Chem.* **2010**, *48* (19), 4296−4309.
(12) Lam, J. W. Y.; Dong, Y.; Kwok, H. S.; Tang, B. Z. Light-Emitting Polyacetylenes: Synthesis and Electrooptical Properties of Poly(1-Phenyl-1-Alkyne)s Bearing Naphthyl Pendants. *Macromolecules* **2006**, *39* (20), 6997−7003.
(13) Ting, C. H.; Hsu, C. S. Photoluminescence and Electroluminescence Characteristics of New Disubstituted Polyacetylenes. *Jpn. J. Appl. Phys.* **2001**, *40*, 5342.
(14) Sun, R.; Zheng, Q.; Zhang, X.; Masuda, T.; Kobayashi, T. Light-Emitting Substituted Polyacetylenes. *Jpn. J. Appl. Phys.* **1999**, *38* (4R), 2017.
(15) Lam, J. W. Y.; Tang, B. Z. Liquid-Crystalline and Light-Emitting Polyacetylenes. *J. Polym. Sci., Part A: polym. Chem.* **2003**, *41* (17), 2607−2629.
(16) Hirohata, M. H. M.; Tada, K. T. K.; Hidayat, R. H. R.; Masuda, T. M. T.; Yoshino, K. Y. K. Effect of Alkyl and Aromatic Substituents on Blue Electroluminescence in Polyacetylene Derivatives. *Jpn. J. Appl. Phys.* **1997**, *36* (3A), L302.
(17) Yu, G.; Liu, Y.; Zhan, X.; Li, H.; Yang, M.; Zhu, D. Thermally Stable Light-Emitting Polymers of Substituted Polyacetylenes. *Thin Solid Films* **2000**, *363* (1), 126−129.
(18) Kim, S. H.; Hur, Y.; Kim, H. S.; Choi, K. H.; Han, Y. S.; Kwak, G.; Kwon, Y.; Park, L. S. Fabrication and Electroluminescence Properties of White OLED with Three-Component, Emitting Layer: Blue and Yellowish-Green Polymers Blend with Red Dopant. *Mol. Cryst. Liq. Cryst.* **2007**, *470* (1), 305−313.
(19) Yang, S. H.; Huang, C. H.; Chen, C. H.; Hsu, C. S. Synthesis and Electroluminescent Properties of Disubstituted Polyacetylene Derivatives Containing Multi-Fluorophenyl and Cyclohexylphenyl Side Groups. *Macromol. Chem. Phys.* **2009**, *210* (1), 37−47.
(20) Ohtsuka, K.; Nagata, S.; Akiya, T. Oxidative Deterioration of Polyacetylene: Its Regulation by Control of Localized Energy Levels. *Synth. Met.* **1987**, *17* (1−3), 289−292.

(21) Billingham, N. C.; Calvert, P. D.; Foot, P. J. S.; Mohammad, F. Stability and Degradation of Some Electrically Conducting Polymers. *Polym. Degrad. Stab.* **1987**, *19* (4), 323−341.
(22) Tsuchihara, K.; Masuda, T.; Higashimura, T. Effects of Ultraviolet Irradiation on Substituted Polyacetylenes. *J. Polym. Sci. A Polym. Chem.* **1991**, *29* (4), 471−478.
(23) Singha, N. R.; Chattopadhyay, P. K.; Deb, M.; Karmakar, M.; Mahapatra, M.; Mitra, M.; Dutta, A. Luminescent Polymer Light-Emitting Devices and Displays. *Polym. Light-Emitting Devices Disp.* **2020**, 125−176.
(24) Skoda, D.; Urbanek, P.; Sevcik, J.; Munster, L.; Antos, J.; Kuritka, I. Microwave-Assisted Synthesis of Colloidal ZnO Nanocrystals and Their Utilization in Improving Polymer Light Emitting Diodes Efficiency. *Mater. Sci. Eng.: B* **2018**, *232*−*235*, 22−32.
(25) Skoda, D.; Urbanek, P.; Sevcik, J.; Munster, L.; Nadazdy, V.; Cullen, D. A.; Bazant, P.; Antos, J.; Kuritka, I. Colloidal Cobalt-Doped ZnO Nanoparticles by Microwave-Assisted Synthesis and Their Utilization in Thin Composite Layers with MEH-PPV as an Electroluminescent Material for Polymer Light Emitting Diodes. *Org. Electron.: Phys., Mater., Appl.* **2018**, *59*, 337.
(26) Donley, C. L.; Zaumseil, J.; Andreasen, J. W.; Nielsen, M. M.; Sirringhaus, H.; Friend, R. H.; Kim, J. S. Effects of Packing Structure on the Optoelectronic and Charge Transport Properties in Poly(9,9-Di-n-Octylfluorene-Alt-Benzothiadiazole). *J. Am. Chem. Soc.* **2005**, *127* (37), 12890−12899.
(27) Noriega, R.; Rivnay, J.; Vandewal, K.; Koch, F. P. V.; Stingelin, N.; Smith, P.; Toney, M. F.; Salleo, A. A General Relationship between Disorder, Aggregation and Charge Transport in Conjugated Polymers. *Nat. Mater.* **2013**, *12* (11), 1038−1044.
(28) Han, K.; Zhou, J.; Li, Q.; Shen, J.; Qi, Y.; Yao, X.; Chen, W. Effect of Filler Structure on the Dielectric and Thermal Properties of SiO2/PTFE Composites. *J. Mater. Sci.: mater. Electron.* **2020**, *31* (12), 9196−9202.
(29) Wang, S.; Xie, S.; Zeng, H.; Du, H.; Zhang, J.; Wan, X. Self-Reporting Activated Ester-Amine Reaction for Enantioselective Multi-Channel Visual Detection of Chiral Amines. *Angew. Chem., Int. Ed.* **2022**, *61* (23), No. e202202268.
(30) Sakaguchi, T.; Shiotsuki, M.; Masuda, T. Synthesis and Properties of Si-Containing Poly(Diarylacetylene)s and Their Desilylated Polymer Membranes. *Macromolecules* **2004**, *37* (11), 4104−4108.
(31) Lee, W. E.; Han, D. C.; Han, D. H.; Choi, H. J.; Sakaguchi, T.; Lee, C. L.; Kwak, G. Remarkable Change in Fluorescence Emission of Poly(Diphenylacetylene) Film via in Situ Desilylation Reaction: Correlation with Variations in Microporous Structure, Chain Conformation, and Lamellar Layer Distance. *Macromol. Rapid Commun.* **2011**, *32* (14), 1047−1051.
(32) Raharjo, R. D.; Lee, H. J.; Freeman, B. D.; Sakaguchi, T.; Masuda, T. Pure Gas and Vapor Permeation Properties of Poly[1-Phenyl-2-[p-(Trimethylsilyl)Phenyl]Acetylene] (PTMSDPA) and Its Desilylated Analog, Poly[Diphenylacetylene] (PDPA). *Polymer* **2005**, *46* (17), 6316−6324.
(33) Jung, H. S.; Verwilst, P.; Kim, W. Y.; Kim, J. S. Fluorescent and Colorimetric Sensors for the Detection of Humidity or Water Content. *Chem. Soc. Rev.* **2016**, *45* (5), 1242−1256.
(34) Kuřitka, I.; Sedlařík, V.; Harea, D.; Harea, E.; Urbánek, P.; Šloufová, I.; Coufal, R.; Zedník, J. Polymer Labelling with a Conjugated Polymer-Based Luminescence Probe for Recycling in the Circular Economy. *Polymers* **2020**, *12* (6), 1226.
(35) Masuda, T. Substituted Polyacetylenes. *J. Polym. Sci. A Polym. Chem.* **2007**, *45* (2), 165−180.
(36) Tsuchihara, K.; Masuda, T.; Higashimura, T. Polymerization of Silicon-Containing Diphenylacetylenes and High Gas Permeability of the Product Polymers1. *Macromolecules* **1992**, *25* (21), 5816−5820.
(37) Tsuchihara, K.; Masuda, T.; Higashimura, T. Tractable Silicon-Containing Poly(Diphenylacetylenes): Their Synthesis and High Gas Permeability. *J. Am. Chem. Soc.* **1991**, *113* (22), 8548−8549.
(38) Schauer, F.; Nádaždy, V.; Gmucová, K. Electrochemical Impedance Spectroscopy for Study of Electronic Structure in Disordered Organic Semiconductors—Possibilities and Limitations. *J. Appl. Phys.* **2018**, *123* (16), 161590.
(39) Nadazdy, V.; Schauer, F.; Gmucova, K. Energy Resolved Electrochemical Impedance Spectroscopy for Electronic Structure Mapping in Organic Semiconductors. *Appl. Phys. Lett.* **2014**, *105* (14), 142109.
(40) Fujiki, M.; Koe, J. R.; Terao, K.; Sato, T.; Teramoto, A.; Watanabe, J. Optically Active Polysilanes. Ten Years of Progress and New Polymer Twist for Nanoscience and Nanotechnology. *Polym. J.* **2003**, *35* (4), 297−344.
(41) Urbánek, P.; Kuřitka, I. Thickness Dependent Structural Ordering, Degradation and Metastability in Polysilane Thin Films: A Photoluminescence Study on Representative σ-Conjugated Polymers. *J. Lumin* **2015**, *168*, 261−268.
(42) Urbanek, P.; Kuritka, I.; Sevcik, J.; Touskova, J.; Tousek, J.; Nadazdy, V.; Nadazdy, P.; Vegso, K.; Siffalovic, P.; Rutsch, R.; Urbanek, M. An Experimental and Theoretical Study of the Structural Ordering of the PTB7 Polymer at a Mesoscopic Scale. *Polymer* **2019**, *169*, 243−254.
(43) Urbánek, P.; Kuřitka, I.; Daniš, S.; Toušková, J.; Toušek, J. Thickness Threshold of Structural Ordering in Thin MEH-PPV Films. *Polymer* **2014**, *55* (16), 4050.
(44) Pelant, I.; Valenta, J. *Luminescence Spectroscopy of Semiconductors*; Oxford Academic, 2012; p 542.
(45) Yoon, K. H.; Park, S. B.; Yang, B. D. Size Effect of Nanoparticles on the Conjugated Polymer in PPV/SiO2 Nanocomposites. *Mater. Chem. Phys.* **2004**, *87* (1), 39−43.
(46) Toy, L. G.; Nagai, K.; Freeman, B. D.; Pinnau, I.; He, Z.; Masuda, T.; Teraguchi, M.; Yampolskii, Y. P. Pure-Gas and Vapor Permeation and Sorption Properties of Poly[1-Phenyl-2-[*p*-(Trimethylsilyl)Phenyl]Acetylene] (PTMSDPA). *Macromolecules* **2000**, *33* (7), 2516−2524.
(47) Tauc, J. Optical Properties and Electronic Structure of Amorphous Ge and Si. *Mater. Res. Bull.* **1968**, *3* (1), 37−46.
(48) Tauc, J.; Grigorovici, R.; Vancu, A. Optical Properties and Electronic Structure of Amorphous Germanium. *Phys. Status Solidi* **1966**, *15* (2), 627−637.
(49) Makuła, P.; Pacia, M.; Macyk, W. How To Correctly Determine the Band Gap Energy of Modified Semiconductor Photocatalysts Based on UV−Vis Spectra. *J. Phys. Chem. Lett.* **2018**, *9* (23), 6814−6817.
(50) Wood, D. L.; Tauc, J. Weak Absorption Tails in Amorphous Semiconductors. *Phys. Rev. B* **1972**, *5* (8), 3144.
(51) Boubaker, K. A Physical Explanation to the Controversial Urbach Tailing Universality. *Eur. Phys. J. Plus* **2011**, *126* (1), 10.
(52) Kurik, M. V. Urbach Rule. *Phys. Status Solidi (A)* **1971**, *8* (1), 9−45.
(53) Ayik, C.; Studenyak, I.; Kranjec, M.; Kurik, M. Urbach Rule in Solid State Physics. *Int. J. Opt. Appl.* **2014**, *4* (3), 76−83.
(54) Kaiser, C.; Sandberg, O. J.; Zarrabi, N.; Li, W.; Meredith, P.; Armin, A. A Universal Urbach Rule for Disordered Organic Semiconductors. *Nat. Commun.* **2021**, *12* (1), 3988.
(55) Kwak, G.; Fukao, S.; Fujiki, M.; Sakaguchi, T.; Masuda, T. Temperature-Dependent, Static, and Dynamic Fluorescence Properties of Disubstituted Acetylene Polymer Films. *Chem. Mater.* **2006**, *18* (8), 2081−2085.
(56) Vohlídal, J.; Graeff, C. F. O.; Hiorns, R. C.; Jones, R. G.; Luscombe, C.; Schué, F.; Stingelin, N.; Walter, M. G. Glossary of Terms Relating to Electronic, Photonic and Magnetic Properties of Polymers (IUPAC Recommendations 2021). *Pure Appl. Chem.* **2022**, *94* (1), 15−69.
(57) Ghasemi, B.; Ševčík, J.; Nádaždy, V.; Végsö, K.; Šiffalovič, P.; Urbánek, P.; Kuřitka, I. Thickness Dependence of Electronic Structure and Optical Properties of F8BT Thin Films. *Polymers* **2022**, *14* (3), 641.
(58) Sevcik, J.; Urbanek, P.; Skoda, D.; Jamatia, T.; Nadazdy, V.; Urbanek, M.; Antos, J.; Munster, L.; Kuritka, I. Energy Resolved-Electrochemical Impedance Spectroscopy Investigation of the Role of

https://doi.org/10.1021/acs.macromol.4c00862
Macromolecules 2024, 57, 7808−7819

Al-Doped ZnO Nanoparticles in Electronic Structure Modification of Polymer Nanocomposite LEDs. *Mater. Des.* **2021**, *205*, 109738.
(59) Zhao, N.; Li, Z.; Qin, L.; Cui, Z.; Sun, Z.; Cheng, Z.; Jiang, C.; Wang, S.; Zhao, T.; Liao, Y.; Wei, B. Lifetime Measurement and Aging Mechanism Analysis of OLED Subpixels. *Displays* **2022**, *75*, 102326.

https://doi.org/10.1021/acs.macromol.4c00862
Macromolecules 2024, 57, 7808−7819